Quantitative detection of umami substances using FT-IR spectroscopy and wavelength optimization

Habib Baraka Omar[1], Yijian Wang[1], Xiaohu Niu[1], Sheng Zhang[1], Guifeng Jia[1,2,3], Ming Zhu[1,2,3], Yaoze Feng[1,2,3,4,5,6*], Douglas Fernandes Barbin[7*]

(1. *College of Engineering, Huazhong Agricultural University, Wuhan 430070, China*;
2. *Key Laboratory of Agricultural Equipment in Mid-lower Yangtze River, Ministry of Agriculture and Rural Affairs, Wuhan 430070, China*;
3. *Key Laboratory of Aquaculture Facilities Engineering, Ministry of Agriculture and Rural Affairs, Wuhan 430070, China*;
4. *Interdisciplinary Sciences Institute, Huazhong Agricultural University, Wuhan 430070, China*;
5. *Shenzhen Institute of Nutrition and Health, Huazhong Agricultural University, Shenzhen 518000, China*;
6. *Shenzhen Branch, Guangdong Laboratory for Lingnan Modern Agriculture, Genome Analysis Laboratory of the Ministry of Agriculture, Agricultural Genomics Institute at Shenzhen, Chinese Academy of Agricultural Sciences, Shenzhen 518120, China*;
7. *School of Food Engineering, University of Campinas – Unicamp, Brazil*)

Abstract: Umami is one of the five basic tastes, primarily represented by monosodium glutamate (MSG) and disodium 5′-inosinate (IMP). The current primary methods for detecting MSG and IMP are expensive and complex, limiting their widespread applications. Hence, there is a need to explore novel and more affordable methods to characterize umami taste substances. FT-IR was used to detect umami substances, MSG, and its mixture with IMP. Uniform spectral spacing method (USS) was combined separately with a continuous projection algorithm (SPA), competitive adaptive weighting algorithm (CARS), and uninformed variable elimination method (UVE) to simplify partial least squares regression (PLSR) and principal component regression (PCR) prediction models. The results demonstrated that the optimal model for MSG solution detection was the USS-CARS-PCR quantitative simplified model based on 17 feature wavelengths with R_c^2=0.97, $RMSE_c$=0.23 g/L, R_p^2=0.96, and $RMSE_p$=0.27 g/L. For MSG and IMP mixture detection, the optimal model was the full wavelength model with R_c^2=0.97, $RMSE_c$=0.11 g/L, R_p^2=0.98, and $RMSE_p$=0.07 g/L. These findings indicate the feasibility of using FT-IR spectroscopy for rapid and quantitative detection of umami substances, providing a theoretical basis for detecting complex umami substances in food using FT-IR technology.

Keywords: disodium 5′-inosinate (IMP), FT-IR, monosodium glutamate (MSG), umami, wavelength selection
DOI: 10.25165/j.ijabe.20261901.9932

Citation: Omar H B, Wang Y J, Niu X H, Zhang S, Jia G F, Zhu M, et al. Quantitative detection of umami substances using FT-IR spectroscopy and wavelength optimization. Int J Agric & Biol Eng, 2026; 19(1): 263–269.

1 Introduction

As the living standard improves, people's pursuit of delightful taste experiences becomes more intense, and the study of umami, one of the five fundamental flavors, has gained prominence. Umami, alongside sour, sweet, bitter, and salty flavors, constitutes a complex realm of taste sensations. However, evaluating umami is more intricate compared to the other four basic tastes due to its multifaceted nature[1]. Umami is particularly complex due to its diverse molecular sources and concentration-dependent and matrix-dependent sensory behaviors. There are differences in the intensity of umami produced by various umami substances[2-4].

Monosodium glutamate (MSG) and disodium inosinate (IMP) are representative umami substances. Numerous studies have reported their synergistic taste enhancement effects in food systems[5,6]. Therefore, the intensity of umami is often measured by the equivalent umami concentration (EUC), which characterizes this synergistic effect between MSG and IMP[7]. To calculate the EUC value, appropriate detection methods are needed to determine the concentrations of MSG and IMP in food.

Currently, quantitative analysis of umami substances still relies primarily on laboratory-based chemical methods such as HPLC, capillary electrophoresis, and continuous chromatography[8]. Lorbetskie et al.[9] employed reversed-phase high-performance liquid chromatography to determine the content of flavored nucleotides in shrimp meat, achieving a standard addition recovery rate of 99.96%-100.34%, with a coefficient of variation ranging from 0.04%-0.4%. Kong et al.[10] prepared chicken broth and chicken hydrolysate to separate and identify the non-volatile umami compounds in chicken. Liu et al.[11] utilized continuous chromatography with sensory evaluation to assess the umami

Received date: 2025-05-23 **Accepted date:** 2025-12-09
Biographies: Habib Baraka Omar, MS, research interest: intelligent detection and control technology, Email: habibzenjboy@gmail.com; **Yijian Wang**, PhD candidate, research interest: intelligent detection and control technology, Email: yijian.wang@webmail.hzau.edu.cn; **Xiaohu Niu**, PhD candidate, research interest: intelligent detection and control technology, Email: liduliduxxh@gmail.com; **Sheng Zhang**, MS, research interest: intelligent detection and control technology, Email: woniukuaipao001@163.com; **Guifeng Jia**, Associate Professor, research interest: agricultural intelligent measurement and control, Email: guifeng@hzau.edu.cn; **Ming Zhu**, Researcher, research interest: modern agricultural development strategies, Email: 13801392760@163.com.
***Corresponding author: Yaoze Feng**, Professor, research interest: intelligent detection and control. College of Engineering, Huazhong Agricultural University, No. 1, Shizishan Street, Hongshan District, Wuhan 430070 China. Tel: +86-27-87282880, Email: yaoze.feng@mail.hzau.edu.cn.; **Douglas Fernandes Barbin**, Professor, research interest: process analytical technologies for food and agricultural products. School of Food Engineering, University of Campinas (UNICAMP), Campinas, Brazil. Tel: +55 (19) 35210070, Email: dfbarbin@unicamp.br

intensity of seven umami-flavor peptides and to characterize their flavor contribution. Although these detection methods achieved high detection accuracy, they require costly instrumentation and involve complex, labor-intensive procedures.

In contrast, vibrational spectroscopy techniques—including FT-IR and NIR—have attracted increasing interest in the field of food organic matter assessment due to their rapid, nondestructive, and reagent-free characteristics. Teixeira et al.[12] obtained near-infrared spectra of powdered wheat and used de-scattering and derivative processing to determine the content of 10 amino acids, predicting the content of leucine and phenylalanine. Wang et al.[13] established a calibration model for the total amount of free amino acids and tea polyphenols in green tea based on near-infrared spectral characteristics, achieving cross-validation standard errors between 0.2300 and 0.2866. Juan et al.[14] used different chemical bonds in α amino acid molecules to characterize and determine their molecular structure through mid-infrared, Raman, and far-infrared absorptions, achieving good results at the B3LYP level. Nevertheless, their work was limited to molecular structure characterization and did not address the quantitative detection of umami substances. Hanim et al.[15] utilized FT-IR to detect anthocyanin content in soybeans, predicting the content of two anthocyanins under different pretreatment methods by screening out 500-800 cm^{-1} bands. These results indicate that it is feasible to detect organic matter in food matrices using FT-IR technology, as the fundamental vibrational frequencies of most chemical bonds are located in the infrared band, especially the characteristic absorption peaks of functional groups[16-20]. However, no studies have yet focused on the quantitative detection of key umami substances using FT-IR spectroscopy, nor have any studies explored the spectral characteristics of MSG–IMP mixed systems, which is crucial for understanding synergistic umami perception. Furthermore, while FT-IR spectra contain abundant chemical information, they also include large amounts of redundant or collinear variables. Previous studies seldom employed comprehensive wavelength-selection frameworks to enhance the efficiency and robustness of umami substance detection. These gaps highlight the need for a rapid, low-cost, and accurate analytical strategy capable of quantifying umami substances and supporting future development of portable taste-evaluation devices.

Therefore, this study aims to investigate the feasibility of using FT-IR spectroscopy for the quantitative detection of umami substances such as MSG and its mixtures with IMP. By combining FT-IR spectroscopy with advanced wavelength selection methods, this research seeks to establish accurate chemometric models based on different preprocessing strategies. In addition, advanced wavelength-selection algorithms are used to simplify the spectral model structure and improve detection efficiency. This work not only fills the current research gap in FT-IR-based umami analysis but also provides methodological guidance for constructing simplified and efficient spectral models suitable for food quality evaluation and intelligent taste-sensing applications.

2 Materials and methods

2.1 Sample preparation and spectrum collection

2.1.1 Reagents and instruments

The monosodium glutamate (MSG) and disodium inosinate (IMP) used in the experiment both with 99% purity were purchased from (Shanghai Yuanye Bio-Technology Co., Ltd, China) and the materials were stored at 4°C for later use. Fourier Transform Infrared (FT-IR) spectrometer (Nicolet IS50, Thermo Scientific Co., Ltd, USA) was employed for spectrum acquisition. The resolution of the instrument was set at 4 cm^{-1} with 16 times scans. The transmission spectra of samples within the wavelength range of 700-4000 cm^{-1} were collected.

2.1.2 MSG solution preparation and spectrum collection

MSG solutions with concentrations of 0.15, 0.3, 0.6, 0.9, 1.2, 1.5, 1.8, 2.1, 2.7, 3.3, 3.9, and 4.5 g/L were prepared respectively. Such a system is hereafter called the simple system. Four replicate samples were prepared for each concentration. Another two batches of experiment were repeated and finally 144 samples were obtained. The prepared sample solutions were placed in 1mm optical path cuvettes for spectrum collection.

2.1.3 Sample preparation for the mixed system

MSG and IMP mixture samples with 12 concentrations were prepared (Table 1). Similar to the MSG solution samples, four replicate samples were prepared for each concentration. The total concentration of each mixed system was 2 g/L. The MSG and IMP concentration ranges were 0.04-1.96 g/L. After repeating twice, a total of 144 samples were obtained. The prepared sample solutions were placed in 1mm optical path cuvettes for spectrum collection.

Table 1 Concentration of MSG and IMP gradient mixing system

IMP/g·L^{-1}	0.04	0.10	0.20	0.40	0.60	0.80	1.00	1.20	1.40	1.60	1.80	1.96
MSG/g·L^{-1}	1.96	1.90	1.80	1.60	1.40	1.20	1.00	0.80	0.60	0.40	0.20	0.04

2.2 Sample set partitioning

In this experiment, the sample set partitioning based on joint *X*-*Y* distances (SPXY) algorithm was employed to divide the dataset into calibration and prediction sets. The SPXY algorithm considers both the spectral variables (*X*) and the corresponding response values (*Y*) when calculating the Euclidean distance between samples, thereby ensuring that the selected subsets represent the overall distribution of both independent and dependent variables[21]. Specifically, samples with the largest joint *X*-*Y* distances were iteratively selected to maximize representativeness and minimize redundancy. In this study, 96 samples were assigned to the calibration set and the remaining 48 samples to the prediction set, maintaining a ratio of 2:1 to balance model training and validation reliability.

2.3 Model calibration and performance evaluation

2.3.1 Spectral preprocessing and characteristic wavelength screening

The spectrum may contain interference information during acquisition. In order to improve the signal-to-noise ratio and obtain a better model, it was necessary to preprocess the original data before establishing calibration models[22]. In this experiment, Savitzky-Golay (SG), multiplicative scatter correction (MSC), standard normal variate (SNV), and mean center (MC) were used[23,24] to pre-process the data.

Due to the large number of full-band variables and possible collinearity, it was necessary to reduce data dimensionality and eliminate irrelevant information before modeling. Therefore, several characteristic wavelength selection algorithms were applied:

Uniform Spectral Spacing (USS)[25]: a simple down-sampling approach that selects spectral variables at equal intervals to reduce data redundancy while maintaining spectral representativeness.

Successive Projections Algorithm (SPA)[26]: a forward selection method that minimizes collinearity by iteratively selecting variables with the smallest projection error in the multidimensional space.

Competitive Adaptive Reweighted Sampling (CARS)[27]: a stochastic sampling strategy that selects variables with high

regression coefficients in Partial Least Squares (PLS) models through exponential decay and adaptive reweighting.

Uninformative Variable Elimination (UVE)[28]: an algorithm that evaluates variable importance based on PLS regression stability, removing those with low signal-to-noise ratios or weak correlations with the response variable.

These algorithms were used in combination to obtain the most informative spectral features for subsequent model calibration.

2.3.2 Modeling method and model evaluation

Partial Least Squares Regression (PLSR)[29] and Principal Component Regression (PCR)[30] were employed for modeling analysis. Coefficient of determination (R^2) and root mean square error (RMSE) were computed as follows to evaluate model performance:

$$R^2 = 1 - \frac{\sum_{i=1}^{N}(\hat{y}_i - y_i)^2}{\sum_{i=1}^{N}(\hat{y}_i - \bar{y}_i)^2} \tag{1}$$

$$\mathrm{RMSE} = \sqrt{\frac{\sum_{i=1}^{N}(\hat{y}_i - y_i)^2}{N}} \tag{2}$$

where, y_i is the actual measured value of the i-th sample, $\hat{y}_i$ is the predicted value of the i-th sample, $\bar{y}_i$ is the average of the measured values of the samples, and N is the number of samples. According to different sample sets, the coefficient of determination R^2 was divided into the coefficient of determination of the calibration set R_c^2 and the coefficient of determination of the prediction set R_p^2. The root mean square error RMSE was divided into the root mean square error of the calibration set RMSE_c and the root mean square error of the prediction set RMSE_p. The higher the R_c^2, R_p^2 of the model and the lower the RMSE_c, RMSE_p were, the better the performance of the model output[31]. For further interpretation of models, we calculated the relative prediction deviation (*RPD*) and the range error ratio (*RER*) as follows:

$$RPD = \frac{SD}{\mathrm{RMSE}_P} \tag{3}$$

$$RER = \frac{Range}{\mathrm{RMSE}_P} \tag{4}$$

where, *SD* is the standard deviation of the reference data; *Range* is the difference between the maximum and minimum values of the reference data; and RMSE_P is the root mean square error of prediction.

According to Williams[32], *RER* values larger than 10 indicate high utility models, and *RPD* values below 1.5 are unreliable for predictions, while 1.5-2.0 can distinguish high from low values. Between 2.0-2.5 allows approximate predictions, 2.5-3.0 is good, and above 3.0 means excellent prediction accuracy, particularly useful for complex and specific applications[33].

3 Results and discussion

3.1 Spectral characteristics of the sample solution

Figure 1a shows the collected spectra of the MSG solution, while Figure 1b presents the spectra of the mixed solution containing MSG and IMP. In both spectra, the absorption band of water molecules was predominant, with a strong and broad peak centered around 3600 cm^{-1} corresponding to the stretching vibration of the O–H bond in water. Due to the aqueous environment, the spectra of the two sample types exhibited similar overall shapes and peak positions.

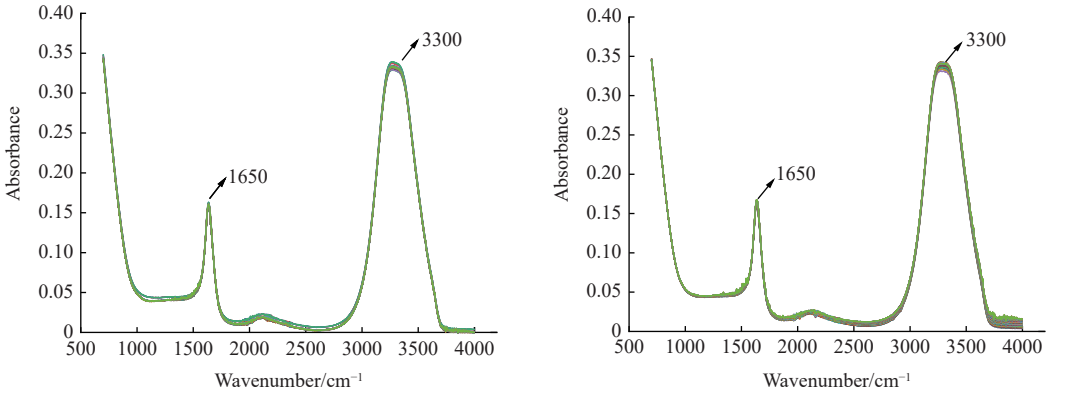

a. MSG single system sample spectrum b. Sample spectrum of mixed solution of MSG and IMP

Figure 1 FT-IR spectrum of sample solution

Several distinct absorption features could be observed in the fingerprint region. The band at approximately 1650 cm^{-1} was attributed to the stretching vibration of the C=O bond, mainly arising from the carboxyl groups in MSG and IMP molecules[34]. The peak at around 3300 cm^{-1} was associated with the N–H stretching vibration, which originates from the amino groups present in both compounds[35]. Furthermore, the weak absorption near 1400 cm^{-1} may correspond to the symmetric stretching of the carboxylate (–COO$^-$) group, indicating interactions between amino and carboxyl groups through intra- or intermolecular hydrogen bonding. These characteristic absorptions reflect the molecular structures of umami substances and provide a theoretical basis for distinguishing solutions with different compositions.

3.2 Influence of pretreatment methods

3.2.1 Selection of spectral pretreatment method for MSG concentration detection in the simple system

Several preprocessing methods are used with Partial Least Squares Regression (PLSR) to detect MSG concentration in a simple system. As listed in Table 2, MC preprocessing yields a weaker prediction with an R_p^2 of 0.88 and higher RMSE_p of 0.47 g/L, making it less effective for prediction compared to others. The model with no preprocessing and the SG preprocessing method yielded the best performance, with R^2 and RMSE of 0.97 and 0.23 g/L, as well as 0.96 and 0.28 g/L for calibration and prediction, respectively. These models also have high *RPD* (4.90) and *RER* (15.51), indicating excellent prediction accuracy and utility. In a

nutshell, the original data (no preprocessing) or SG preprocessing are the best models for MSG detection in the simple system, as both provide high accuracy and minimal error with simple data processing steps.

Table 2 Performance of PLSR models for MSG concentration detection based on different pre-treatment methods

Pre-treatment method	R_c^2	RMSE$_c$/ g·L^{-1}	R_p^2	RMSE$_p$/ g·L^{-1}	*RPD*	*RER*
None	0.97	0.23	0.96	0.28	4.90	15.51
SG	0.97	0.23	0.96	0.28	4.90	15.51
MSC	0.96	0.27	0.93	0.37	3.71	11.74
MC	0.97	0.23	0.88	0.47	2.92	9.24
SNV	0.96	0.27	0.93	0.37	3.71	11.74

Note: None: No preprocessing is applied to the data; SG (Savitzky-Golay): Smooths the data to reduce noise; MSC (Multiplicative Scatter Correction): Corrects for light scattering effects; MC (Mean Centering): Averages the data around the mean; SNV (Standard Normal Variate): Normalizes the spectra for comparison.

3.2.2 Selection of spectral pretreatment method for MSG concentration detection in mixed system

The same preprocessing methods (None, SG, MSC, MC, SNV) are applied to detect MSG concentration in a mixed system containing both MSG and IMP. Because the total concentration of MSG and IMP in each gradient sample was invariant, this experiment chose MSG as an indicator for the detection of umami substances in the mixed system. The corresponding PLSR full-wavelength models were established respectively based on the spectral data preprocessed by different methods. The model results are listed in Table 3.

Table 3 PLSR model results for MSG concentration detection in mixed system based on different pretreatment methods

Pre-treatment method	R_c^2	RMSE$_c$/ g·L^{-1}	R_p^2	RMSE$_p$/ g·L^{-1}	*RPD*	*RER*
None	0.97	0.11	0.98	0.07	8.29	27.43
SG	0.97	0.11	0.98	0.08	7.25	24.00
MSC	0.97	0.10	0.98	0.06	9.67	32.00
MC	0.97	0.11	0.91	0.19	3.05	10.11
SNV	0.98	0.10	0.97	0.06	9.67	32.00

It can be seen from Table 3 that the performances of the models established by the original and preprocessing data were all robust, and the R^2 of the prediction set were all above 0.90. However, it was also found that the preprocessing method did not necessarily improve the performance of the model. The predictive coefficient of determination R_p^2 of the model established by MC preprocessing was slightly lower than that of the original model. Besides, the performance of the models established by other preprocessing methods was equivalent to the one established by the original data, in which the coefficient of determination and the root mean square errors were not 1.00% greater or lower than those of the original data model, respectively. In particular, the models with MSC and SNV preprocessing outperform the others, with R_p^2= 0.98 and RMSE$_p$ = 0.06 g/L, indicating very high predictive accuracy. The MSC model also shows the highest *RPD* (9.67) and *RER* (32.00), indicating excellent prediction performance, particularly useful for detecting umami substances in complex systems. As preprocessing increases the workloads, the None preprocessing model also performs well where the coefficient of determination and the root mean square error of the calibration set and prediction set were R_c^2=0.97, RMSE$_c$=0.11 g/L, R_p^2=0.98, and RMSE$_p$=0.07 g/L, respectively, though slightly worse than the MSC and SNV models. All in all, MSC preprocessing is the most outstanding model for the mixed system of MSG and IMP, as it provides the highest *RPD* and *RER* values, indicating excellent accuracy and reliability in predicting MSG concentration in a mixed system.

3.3 Establishment and comparison of simplified detection models

3.3.1 Preliminary dimensionality reduction of spectral data

The FT-IR spectral data of samples had a large dimension with 6846 wavelengths, where redundant data were inevitably included, making the model structure complex. When directly using SPA, CARS, or UVE characteristic wavelength selection, the calculation was lengthy and time-consuming, which seriously deteriorated the modeling performance. In this experiment, USS was utilized to preliminarily reduce the dimensionality of the spectral variables. Then the second wavelength selections were performed to further simplify model structure and reduce calculations under the premise of ensuring the performance of models. USS selects effective bands by changing the step length, that is, extracting new spectral data at intervals of 1, 2, 3, 4, 5...100 to establish PLSR models. The root mean square errors of the prediction set RMSE$_p$ of all models were analyzed.

As shown in Figure 2a, in the detection of a single MSG system, when the number of intervals is 25, the model yielded the best performance with 274 extracted wavelengths, where RMSE$_p$ is as low as 0.19 g/L, lower than the 0.28 g/L of the full-wavelength model. In the detection of the mixed system of MSG and IMP, as shown in Figure 2b, when the number of intervals is 54, the model had the best performance with 127 extracted wavelengths, and the corresponding RMSE$_p$ is 0.09 g/L, slightly higher than the 0.07 g/L of the full-wavelength detection model. In both the single system and the mixed system, the detection model based on USS only can effectively reduce the data dimension, simplify the algorithm complexity, and improve the performance of the model[36].

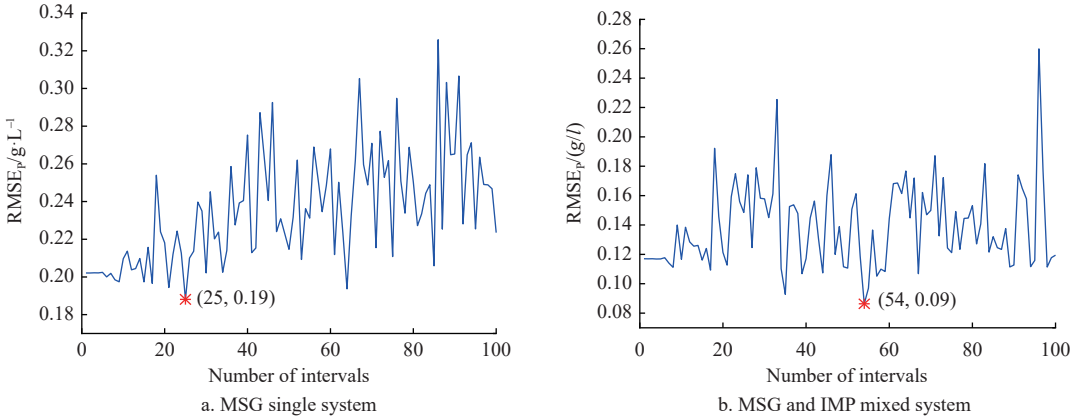

a. MSG single system b. MSG and IMP mixed system

Figure 2 Preliminary variable selection by USS for MSG concentration detection

FT-IR spectroscopy detects umami substances by selecting the most effective wavelengths. Figure 2 above shows examples of how different numbers of intervals and corresponding errors might affect umami detection: 54 intervals with an error of 0.091 has a higher number of intervals, indicating more data points or wavelengths are being used in the model, resulting in an error of 0.091. This suggests that the model is more precise but likely more complex due to the larger number of intervals. 35 intervals implies that fewer intervals generally lead to higher errors. The exact error would depend on the dataset and how well these intervals capture the essential features. 15 intervals with an error perhaps of 0.10 represents a simpler model with fewer data points, which increases the error to 0.10. This trade-off suggests a loss in precision but a significant gain in model simplicity and possibly computational efficiency.

3.3.2 Establishment of simplified models for MSG concentration detection in the simple system

Wavelengths screened by USS, SPA, CARS, and UVE were used to further select characteristic wavelengths respectively. Then PLSR and PCR models were established to compare the effects of different characteristic wavelength selection methods (Table 4).

It can be seen from Table 4 that the models based on characteristic wavelengths performed well in the simple systems, where the prediction coefficients of determination were all greater than 0.93, and the root mean square error of the prediction set was less than 0.35 g/L, slightly lower than that of full-wavelength detection models with $RMSE_p$ and R_p^2 of 0.28 g/L and 0.96. In addition, compared with the model based on USS only with $RMSE_p$ of 0.19 g/L, the simplified model had a higher $RMSE_p$. Nevertheless, all the models developed were proven to be excellent with RPD>3 and of high utility value with RER >10.

Table 4 PLSR and PCR model results for MSG concentration detection in the simple system established by different wavelength selection methods

Modeling method	Wavelength selection	Number of variables	R_c^2	$RMSE_c$/ g·L^{-1}	R_p^2	$RMSE_p$/ g·L^{-1}	*RPD*	*RER*
PLSR	USS-CARS	17	0.96	0.25	0.94	0.33	4.18	13.15
	USS-UVE	35	0.95	0.30	0.96	0.28	4.93	15.50
	USS-SPA	12	0.96	0.25	0.96	0.28	4.93	15.50
PCR	USS-CARS	17	0.97	0.23	0.96	0.27	5.11	16.07
	USS-UVE	35	0.96	0.27	0.94	0.33	4.18	13.15
	USS-SPA	12	0.96	0.28	0.94	0.33	4.18	13.15

However, in general, characteristic wavelength selection greatly reduced the model variables and ensured an excellent model. The PCR with USS-CARS model shows the highest R^2, *RPD*, *RER* and lowest RMSE values, indicating it is the most reliable and has the best prediction accuracy among the models listed.

Figure 3a shows the scatter plot of the true and predicted values of the calibration set and prediction set of the optimal model (USS-CARS-PCR). The coefficient of determination and the root mean square error were R_c^2 = 0.97, $RMSE_c$=0.23 g/L, and R_p^2=0.96, $RMSE_p$ =0.27 g/L, respectively. Figure 3b shows the visualization process of CARS variables selection, where the Monte Carlo coefficient was set to 100. It can be seen from Figure 3b that the number of selected variables decreased rapidly with the increase in the number of iterations (Figure 3b). However, the value of $RMSE_{cv}$ first decreased and then increased (Figure 3b), indicating that useful information was eliminated at the later stage of the iteration.

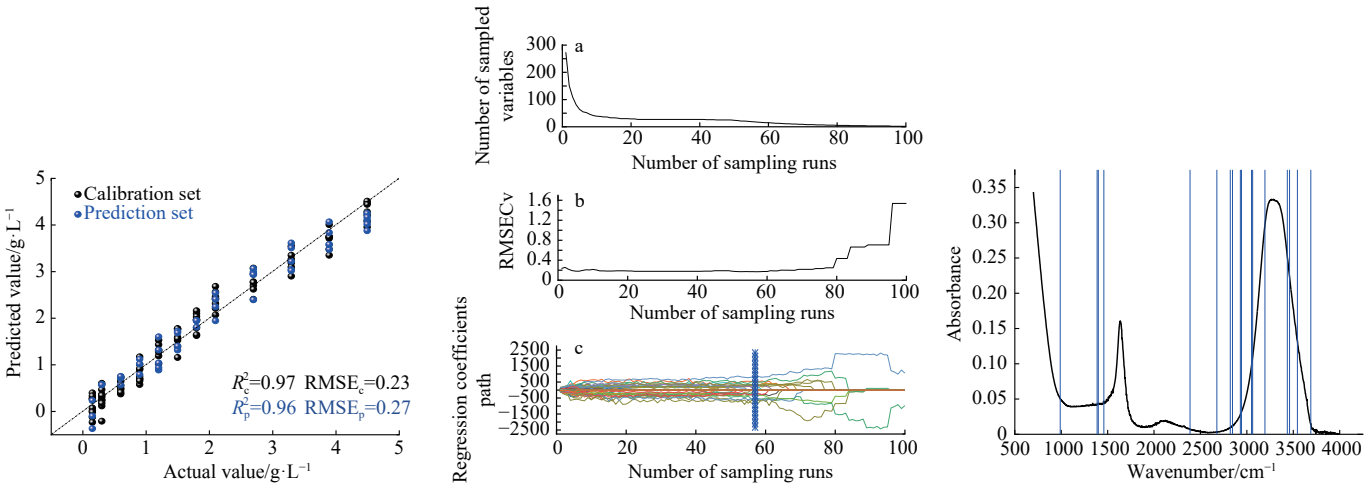

a. Scatter plot of MSG concentration detection data model verification in a single system

b. Process of selecting wavelength variables by CARS method

c. CARS feature wavelength selection

Figure 3 MSG single system test model effect

When the number of iterations was 57 (asterisk dot position), the value of $RMSE_{cv}$ was the smallest. Within that point, the corresponding band number was 17, which occupied only 0.83% of the original number of wavelengths. The distribution of characteristic wavelengths is shown in Figure 3c, including 989.3, 1387.1, 1399.1, 1459.4, 2387.4, 2676.7, 2821.3, 2845.5, 2929.8, 2941.9, 3050.4, 3062.4, 3195.0, 3436.0, 3460.2, 3544.5, and 3689.2 cm^{-1}. The wavelengths number corresponding to the characteristic wavelength was mainly between 1300-1660, 2550-3000, and 3250-3550 cm^{-1}, of which 1300-1660 cm^{-1} corresponded to CN and C=O bond stretching vibration[37]; 2550-3000 cm^{-1} corresponded to R-COOH functional group stretching vibration (4136)[38]; 3250-3550 cm^{-1} corresponded to NH_2 stretching vibration [39].

3.3.3 Establishment of simplified model for MSG concentration detection in mixed system

Wavelength selection was performed by USS, SPA, CARS, and UVE, and PLSR and PCR models were established to compare the effects of different characteristic wavelength selection methods (Table 5). The results show that the coefficients of determination for prediction of the MSG concentration detection model established based on different characteristic wavelength selection methods in the mixed system were all above 0.94, which was slightly lower

than that of the original data model. The prediction root mean square error was less than 0.14 g/L, slightly higher than the original data model. Although the performance of all the models is slightly inferior to that of the original data model, the number of model variables was greatly reduced, and the variable compression rate was more than 1:500, which means a crucial drop in complexity. In general, the PLSR model based on USS-CARS characteristic wavelength selection had the best performance with the highest coefficient of determination R_c^2=0.94 and R_p^2=0.96 and the lowest root mean square error $RMSE_c$=0.17 g/L, $RMSE_p$=0.12 g/L.

Figure 4a presents the scatter plot of the true value and predicted value of the calibration set and prediction set of the optimal model (USS-CARS-PLSR). The distribution of characteristic wavelengths is shown in Figure 4b, including 1403.0, 1689.3, 1741.4, 1793.5, 1819.5, 1871.6, 2600.5, and 2782.8 cm^{-1}. The wavelength numbers corresponding to the selected characteristic wavelengths were mainly concentrated in 1550-1900 and 2600-2800 cm^{-1}. Some major peaks were observed, where 1550-1900 cm^{-1} corresponded to the C=O bond stretching vibration in the carbonyl group [40], and 2600-2800 cm^{-1} corresponded to the P-O stretching vibration in IMP[41].

Table 5 PLSR and PCR model results of MSG concentration detection in a mixed system established by employing different wavelength selection methods

Modeling method	Wavelength selection	Number of variables	R_c^2	$RMSE_c$/ g·L^{-1}	R_p^2	$RMSE_p$/ g·L^{-1}	*RPD*	*RER*
PLSR	USS-CARS	8	0.94	0.17	0.96	0.12	4.92	16.00
	USS-UVE	13	0.90	0.20	0.96	0.12	4.92	16.00
	USS-SPA	8	0.90	0.21	0.95	0.12	4.92	16.00
PCR	USS-CARS	8	0.93	0.17	0.96	0.12	4.92	16.00
	USS-UVE	13	0.90	0.21	0.96	0.12	4.92	16.00
	USS-SPA	8	0.90	0.21	0.95	0.13	4.54	14.77

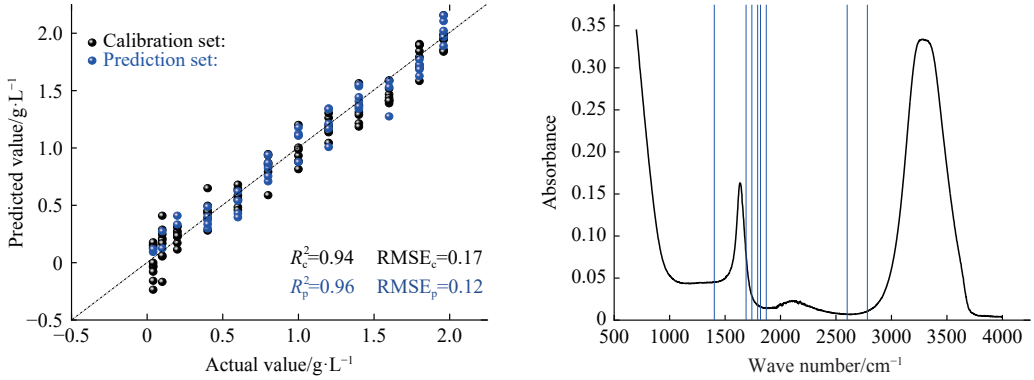

a. Scatter plot of MSG concentration detection data model verification in mixed system

b. CARS feature wavelength selection

Figure 4 MSG and IMP mixture detection model effect

4 Conclusions

In the current study, the feasibility of using FT-IR spectroscopy for the quantitative identification of umami substances in solution was demonstrated. Both the MSG single system and its mixed system with IMP were investigated to evaluate spectral responses and establish quantitative models. Among the tested chemometric approaches, PLSR and PCR models based on original or pre-processed spectra exhibited high prediction accuracy, confirming the potential of FT-IR spectroscopy for umami substance quantification. It was observed that the choice of preprocessing methods had system-dependent effects: for the simple MSG system, models built on raw or SG-preprocessed data yielded optimal performance, whereas for the mixed MSG–IMP system, the MSC-preprocessed model provided the most reliable predictions. Furthermore, the combination of uniform spectral spacing (USS) and advanced wavelength selection algorithms (SPA, CARS, and UVE) effectively reduced data dimensionality, achieving wavelength compression ratios exceeding 1:400 without compromising predictive capability. The USS–CARS–PCR model, which utilized only 17 wavelengths with a compression ratio above 1:500, proved to be the most efficient and accurate for MSG detection. These results demonstrate the practicality of FT-IR spectroscopy coupled with chemometric modeling for rapid, low-cost, and non-destructive detection of umami substances.

Methodological strengths of this study include the use of systematic wavelength screening to minimize redundant spectral information, the comparative evaluation of multiple preprocessing and modeling techniques, and the establishment of a simplified yet robust spectral model suitable for real-time detection. Limitations, however, remain in that the experiments were conducted under controlled solution conditions, and matrix effects commonly encountered in real food systems were not fully addressed. In addition, the current study primarily focused on two representative umami substances, and the generalizability to broader compound categories requires further verification. Future research should focus on extending the proposed method to complex food matrices, developing portable FT-IR systems for on-site detection, and integrating spectral analysis with machine learning or bionic sensing technologies to achieve intelligent, multi-dimensional evaluation of umami perception.

Acknowledgements

This study was supported by Key Research and Development Program of Hubei Province (Grant No. 2023BBB038), Fundamental Research Funds for the Central Universities (Grant No. 107/11041910104; 2662020GXPY003), and HZAU-AGIS Cooperation Fund (Grant No. SZYJY2022028). Mr. Tao Yuan and Haopeng Liu are highly appreciated for their kind assistance during experiments.

[References]

[1] Zhao Y G, Zhang M, Devahastin S, Liu Y. Progresses on processing methods of umami substances: A review. Trends Food Sci. Technol., 2019; 93(1): 125–135.

[2] Harada-Padermo S d S, Dias-Faceto L S, Selani M M, Alvim I D, Floh E I S, Macedo A F, et al. Umami Ingredient: Flavor enhancer from shiitake

(*Lentinula edodes*) byproducts. Food Res. Int., 2020; 137: 109540.
[3] Zhang N L, Wang W L, Li B, Liu Y. Non-volatile taste active compounds and umami evaluation in two aquacultured pufferfish (*Takifugu obscurus* and *Takifugu rubripes*). Food Biosci., 2019; 32: 100468.
[4] Wang W L, Zhou X R, Liu Y. Characterization and evaluation of umami taste: A review. TrAC-Trends Anal. Chem., 2020; 127: 115876.
[5] Nishimura T, Goto S, Miura K, Takakura Y, Egusa A S, Wakabayashi H. Umami compounds enhance the intensity of retronasal sensation of aromas from model chicken soups. Food Chem., 2016; 196: 577–583.
[6] Yang J, Huang Y R, Cui C, Dong H, Zeng X F, Bai W D. Umami-enhancing effect of typical kokumi-active γ-glutamyl peptides evaluated via sensory analysis and molecular modeling approaches. Food Chem., 2021; 338: 128018.
[7] Kong L Q, Hong F, Luan P, Chen Y P, Feng Y Z, Zhu M. Novel competitive electrochemical impedance biosensor for the ultrasensitive detection of umami substances based on Pd/Cu-TCPP(Fe). Food Chem., 2024; 438: 137631.
[8] Zhang Y, Gao X C, Pan D D, Zhang Z G, Zhou T Q, Dang Y L. Isolation, characterization and molecular docking of novel umami and umami-enhancing peptides from *Ruditapes philippinarum*. Food Chem., 2021; 343: 128522.
[9] Lorbetskie B, White T, Creskey M, Zhang X, Girard M, Tam R Y, et al. Selective reversed-phase high-performance liquid chromatography method for the determination of intact SARS-CoV-2 spike protein. J. Chromatogr. A, 2022; 1680: 463424.
[10] Kong Y, Yang X, Ding Q, Zhang Y Y, Sun B G, Chen H T, et al. Comparison of non-volatile umami components in chicken soup and chicken enzymatic hydrolysate. Food Res. Int., 2017; 102: 559–566.
[11] Liu Z Y, Zhu Y W, Wang W L, Zhou X R, Chen G L, Liu Y. Seven novel umami peptides from *Takifugu rubripes* and their taste characteristics. Food Chem., 2020; 330: 127204.
[12] Teixeira A, Blasco J, Aleixos-borr N, Barbin D F. Near infrared techniques applied to analysis of wheat-based products: Recent Advances and Future Trends. Food Control, 2022; 140: 109115.
[13] Wang J H, Wang Y F, Cheng J J, Wang J, Sun X D, Sun S, et al. Enhanced cross-category models for predicting the total polyphenols, caffeine and free amino acids contents in Chinese tea using NIR spectroscopy. LWT-Food Science and Technology, 2018; 96: 90–97.
[14] Moreno J R A, Moreno M D M Q, Ureña F P, González J J L. Conformational preference of short aromatic amino acids from the FT-IR, FT-Raman and Far-IR spectroscopies, and quantum chemical calculations: L-phenylalanine and l-tyrosine. Tetrahedron Asymmetry, 2012; 23(14): 1084–1092.
[15] Amanah H Z, Joshi R, Masithoh R E, Choung M-G, Kim K-H, Kim G, et al. Nondestructive measurement of anthocyanin in intact soybean seed using Fourier Transform Near-Infrared (FT-NIR) and Fourier Transform Infrared (FT-IR) spectroscopy. Infrared Phys. Technol., 2020; 111: 103477.
[16] Zhang G, Sun F L, Li H C, Lin Y X, Zhao K, Fang L. The content and emission form of volatile organic compounds from cooking oils: A gas chromatography-mass spectrometry (GC-MS) analysis. Int. J. Environ. Res. Public Health, 2023; 20(3). doi: 10.3390/ijerph20031796.
[17] Kong L Q, Wang Y J, Shu G Q, Wang R F, Feng Y Z, Zhu M. Kinetics of a new porcine taste-bud tissue biosensor for the detection of umami substances and their synergistic effect. Biosens. Bioelectron., 2022; 210: 114304.
[18] Albuquerque N, Meehan B, Hughes J, Surapaneni A. Determination of total carbon in biosolids using MID-infrared spectroscopy. Sci. Total Environ., 2020; 698: 134195.
[19] Gordon R, Chapman J, Power A, Chandra S, Roberts J, Cozzolino D. Mid-infrared spectroscopy coupled with chemometrics to identify spectral variability in Australian barley samples from different production regions. J. Cereal Sci., 2019; 85: 41–47.
[20] Tian H, Zhang L N, Li M, Wang Y, Sheng D G, Liu J, et al. Weighted SPXY method for calibration set selection for composition analysis based on near-infrared spectroscopy. Infrared Phys. Technol., 2018; 95: 88–92.
[21] Clua-Palau G, Jo E, Nikolic S, Coello J, Maspoch S. Finding a reliable limit of detection in the NIR determination of residual moisture in a freeze-dried drug product. J. Pharm. Biomed. Anal., 2020; 183: 113163.
[22] Feng Y Z, Elmasry G, Sun D W, Scannell A G, Walsh D, Morcy N. Near-infrared hyperspectral imaging and partial least squares regression for rapid and reagentless determination of *Enterobacteriaceae* on chicken fillets. Food Chem., 2013; 138(2-3): 1829–1836.
[23] Li C, Zhao T L, Li C, Mei L, Yu E, Dong Y T, et al. Determination of gossypol content in cottonseeds by near infrared spectroscopy based on Monte Carlo uninformative variable elimination and nonlinear calibration methods. Food Chem., 2017; 221: 990–996.
[24] Zhao H T, Feng Y Z, Chen W, Jia G F. Application of invasive weed optimization and least square support vector machine for prediction of beef adulteration with spoiled beef based on visible near-infrared (Vis-NIR) hyperspectral imaging. Meat Sci., 2019; 151: 75–81.
[25] Wang J, Tang C, Li Z L, Liu X W, Zhang W, Zhu E, et al. Hyperspectral band selection via region-aware latent features fusion based clustering. Inf. Fusion, 2022; 79: 162–173.
[26] Mu K X, Feng Y Z, Chen W, Yu W. Near infrared spectroscopy for classification of bacterial pathogen strains based on spectral transforms and machine learning. Chemom. Intell. Lab. Syst., 2018; 179: 46–53.
[27] Liu X, Zhang X, Rong Y Z, Wu J H, Yang Y J, Wang Z W. Rapid determination of fat, protein and amino acid content in coix seed using near-infrared spectroscopy technique. Food Anal. Methods, 2015; 8(2): 334–342.
[28] Kang Z L, Zhao Y C, Chen L, Guo Y J, Mu Q S, Wang S Y. Advances in machine learning and hyperspectral imaging in the food supply chain. Food Eng. Rev., 2022; 14(4): 596–616.
[29] Chen W, Feng Y Z, Jia G F, Zhao H T. Application of artificial fish swarm algorithm for synchronous selection of wavelengths and spectral pretreatment methods in spectrometric analysis of beef adulteration. Food Anal. Methods, 2018; 11: 2229–2236.
[30] Sun C Y, Yin Y Z, Kang H B, Ma H J. A distributed principal component regression method for quality-related fault detection and diagnosis. Inf. Sci. (Ny), 2022; 600: 301–322.
[31] Wang W, Lu Y. Analysis of the mean absolute error (MAE) and the root mean square error (RMSE) in assessing rounding model. IOP Conf. Ser. : Mater. Sci. Eng, 2018; 324: 012049.
[32] Font R, del Río-Celestino M, de Haro-Bailón A. Near-infrared reflectance spectroscopy. Methods in Biotechnology, 2007; 23: 205–217.
[33] Saeys W, Mouazen A M, Ramon H. Potential for onsite and online analysis of pig manure using visible and near infrared reflectance spectroscopy. Biosyst. Eng., 2005; 91: 393–402.
[34] Zeng J, Guo Y, Han Y Q, Li Z M, Yang Z X, Chai Q Q, et al. A review of the discriminant analysis methods for food quality based on near-infrared spectroscopy and pattern recognition. Molecules, 2021; 26(3). doi: 10.3390/molecules26030749.
[35] Wang X, Huang J H, Fan W, Lu H M. Identification of green tea varieties and fast quantification of total polyphenols by near-infrared spectroscopy and ultraviolet-visible spectroscopy with chemometric algorithms. Anal. Methods, 2015; 7(2): 787–792.
[36] Li M T, Sun D, Liu S B, Zhao R, Zhang K Q. Construction of rapid prediction models for TN and TP in dairy farms slurry under different seasons by near infrared spectroscopy. Spectrochim. Acta - Part A Mol. Biomol. Spectrosc., 2024; 305: 123517.
[37] Feng Y Z, Yu W, Chen W, Peng K K, Jia G F. Invasive weed optimization for optimizing one-agar-for-all classification of bacterial colonies based on hyperspectral imaging. Sensors Actuators, B Chem., 2018; 269: 264–270.
[38] Zhu H Q, Zhao H R, Wei H Y, Wang W, Wang H R, Li K, et al. Investigation into the thermal behavior and FTIR micro-characteristics of re-oxidation coal. Combust and Flame, 2020; 216: 354–368.
[39] Hansen P E, Vakili M, Kamounah F S, Spanget-Larsen J. NH stretching frequencies of intramolecularly hydrogen-bonded systems: An experimental and theoretical study. Molecules, 2021; 26: 24.
[40] Pitsevich G A, Kozlovskaya E, Doroshenko I. Analysis of the carbonyl group stretching vibrations in some structural fragments of poly-3-hydroxybutyrate. arXiv:1604.00815, 2016. DOI: 10.48550/arXiv.1604.00815
[41] Rammah Y S, El-Agawany F I, Mahmoud K A, El-Mallawany R, Ilik E, Kilic G. FTIR, UV–Vis–NIR spectroscopy, and gamma rays shielding competence of novel ZnO-doped vanadium borophosphate glasses. J. Mater. Sci. Mater. Electron., 2020; 31(12): 9099–9113.